PERGAMON International Journal of Non-Linear Mechanics 37 (2002) 1147–1161

INTERNATIONAL JOURNAL OF
NON-LINEAR
MECHANICS

www.elsevier.com/locate/ijnonlinmec

Kelvin–Voigt versus Bürgers internal damping in modeling of axially moving viscoelastic web

Krzystof Marynowski *, Tomasz Kapitaniak

Division of Dynamics, Technical University of Łódź, Stefanowskiego 1/15, 90-924 Łódź, Poland

Abstract

Stability and oscillation characteristics of two-dimensional axially moving web have been investigated. The application of one-dimensional beam-like models of the web allows the identification of instability regions and the estimation of the critical speed. For the beam material two different models, i.e., Kelvin–Voigt and Bürgers have been considered. The numerical solutions of full non-linear and linearized equations have been compared. The effects of axially travelling speed and the internal damping on dynamical stability of axially moving web have been studied in details. Our numerical studies of Kelvin–Voigt and Burger's models show that both models give similar results for small values of internal damping and can be used to describe the dynamics of axially moving webs made from materials with internal damping coefficient smaller than 3×10^{-5}. For the materials with larger damping coefficient the Bürgers model gives more reliable results.

Keywords: Moving web; Internal damping; Dynamic stability

1. Introduction

The continuous development of mechanics and its engineering applications in our days have increased remarkably the interest in non-linear stability analysis of structures. Particularly a great number of studies consider two general models, the systems under followed loading [1–10] and elastic continua translating at high speed [11–20]. In the following dynamical behavior of the second model is studied.

Elastic continua translating at high speed such as band saw blades, magnetic types, paper webs, plastic sheets, films, transmission cables are present in various industrial applications. Generally, axially moving continuum in the form of thin, flat rectangular shape material with small flexural stiffness is called a web. Webs are moving at high speed, for example, in paper production the paper webs are transported with longitudinal speeds of up to 3000 m/min. Above the critical speed one can expect various dynamical instabilities mainly of divergent and flutter type. These instabilities can decrease the quality of products and their performance. The excessive oscillations of a computer tape degrade the signal and can affect the data storage. The instability of a band saw results in low surface quality, unsatisfactory cutting performance and leads to the loss of raw materials. In paper production, the machines instabilities, resonance oscillations and the flutter of the web can cause the wrinkling or even a breaking of the web. To ensure that the operating system is under stable working conditions, full analysis of its dynamics has to be performed. Complete knowledge of the dynamical

* Corresponding author.
E-mail address: kmarynow@ck-sg.p.lodz.pl (K. Marynowski).

0020-7462/02/$ - see front matter
PII: S0020-7462(01)00142-1

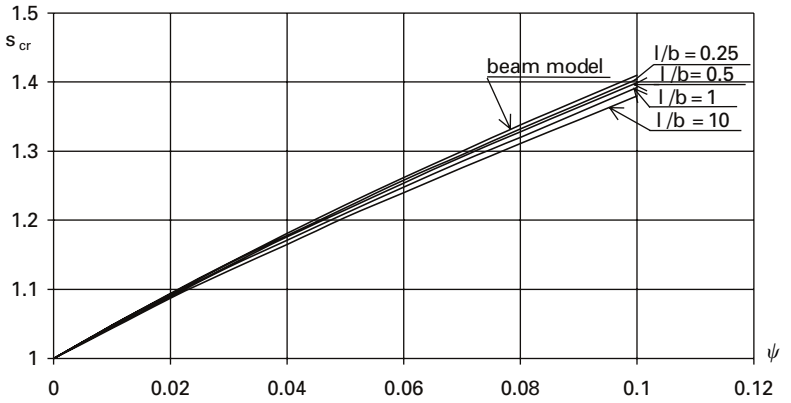

Fig. 1. Critical speeds s_{cr} versus dimensionless stiffness ψ for various webs [20].

behavior allows the prediction and control of instabilities.

The results of the dynamical analysis of the axially moving web shows that it is impossible to obtain the mathematical model, which is valid for the whole range of transport speeds. It has been necessary to introduce a number of simplifications in the considered models. The validation of such models is restricted to specific intervals of transport speed and usually they describe only the most significant features of the dynamical behavior.

In modeling the axially moving webs one can use one-dimensional beam theory (e.g. [24]) or two-dimensional plate theory (e.g. [20]). Historically, also the string theory has been used but nowadays it is considered to give too rough approximation of the real phenomena as it has not considering plate stiffness of the web. Although the plate theory gives the most accurate description of the physical phenomena that occur in the web, it is very complicated mathematically and requires time-consuming calculations. Our previous studies show that for the large class of the practically important webs with small flexural stiffness the beam theory gives equally accurate results as the plate theory [20]. In particular, the plot of critical speed s_{cr} of the web (defined as the ratio of the transport speed to the wave speed) versus dimensionless plate stiffness ψ (defined as $Eh^3/[12(1-\nu^2)Pl^2]$) is shown in Fig. 1.

One can observe that for the large range of stiffness ψ and the slenderness ratio l/b (length over width of the web) the results of the beam and the plate theories are very close.

The other important problem one can meet in considering axially moving web is how to model web material. Particularly, how to model the internal damping of the material and this is the main problem, which we stress in this paper. Generally, two different models, namely Kelvin–Voigt [22] and Bürgers [23] are commonly used and we try to answer the question, which of them better describes the dynamics of the web. Additionally, we compare the results obtained from the analysis of the linearized equations with the results of the integration of the full non-linear equations.

The paper is organized as follows. In Section 2 basing on the beam theory, we derive the equations of motion of the axially moving web. Section 3 describes differential constitutive equations obtained from two-parameter Kelvin–Voigt and four parameter Bürgers models. In Section 4 we give full mathematical models of the web with Kelvin–Voigt (Section 4.1) and Bürgers damping (Section 4.2). In Section 5, we discuss the results of our numerical investigations of two-parameter Kelvin–Voigt (Section 5.1) and four-parameter Bürgers (Section 5.2) models. The conclusions are presented in Section 6.

2. Equations of motion

A viscoelastic axially moving web of the length l is considered. The web moves at axial velocity c. The

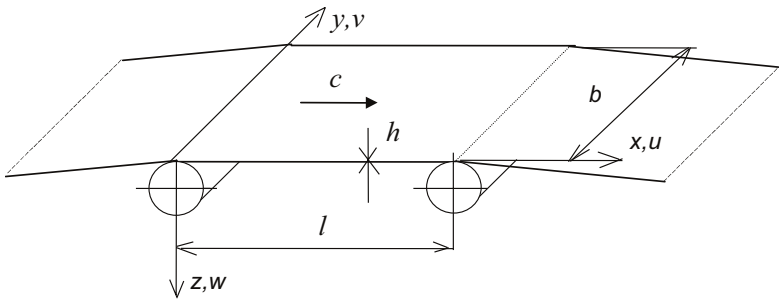

Fig. 2. Axially moving web.

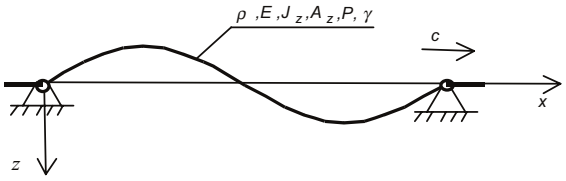

Fig. 3. The beam model of axially moving web.

geometry of the system and the introduced co-ordinates are shown in Fig. 2.

The problem of transverse oscillations of the axially moving continua in a state of uniform initial stress was investigated [20]. In the case of thin web, the results of earlier studies show that the beam models can approximate the dynamical behavior of the web (Fig. 3). The application of this model gives the following equation of motion in the z direction:

$$\rho A_z(-w_{,tt} - 2cw_{,xt} - c^2 w_{,xx}) + M_{x,xx} + (N_x w_{,x})_{,x} = 0, \tag{1}$$

where: A_z the cross section area of the beam, M_x bending moment, N_x perturbated axial stress, ρ mass density of the beam.

The uniform initial tension force P provides the required initial stress for the models' materials. The non-linear strain component in x direction is related to the displacement w by

$$\varepsilon(x,t) = \tfrac{1}{2} w_{,x}^2(x,t). \tag{2}$$

The one-dimensional constitutive equation of a differential type material obeys the relation

$$\Gamma\sigma = \Xi\varepsilon, \tag{3}$$

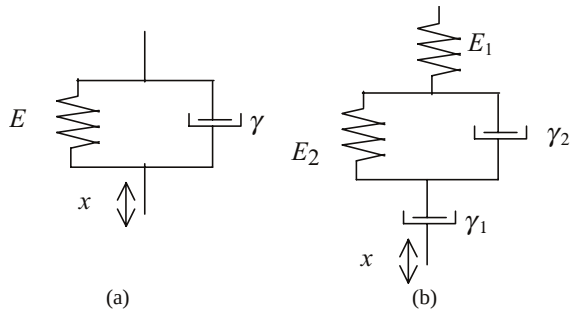

Fig. 4. (a) Kelvin–Voigt and (b) Bürgers models.

where Γ and Ξ are differential operators defined as

$$\Gamma = \sum_{j=0}^{R} a_j \frac{\mathrm{d}^j}{\mathrm{d}t^j}, \quad \Xi = \sum_{j=0}^{P} b_j \frac{\mathrm{d}^j}{\mathrm{d}t^j}. \tag{4}$$

3. Differential constitutive equations

The models of internal damping introduced by Kelvin–Voigt and Bürgers are shown in Fig. 4.

For the two-parameter viscoelastic model of material—Kelvin–Voigt element (Fig. 4a), the differential constitutive equation can be written as

$$a_0\sigma = b_1\varepsilon_{,t} + b_o\varepsilon, \tag{5}$$

where

$$a_0 = 1, \quad b_0 = E, \quad b_1 = \gamma. \tag{6}$$

The four-parameter viscoelastic model of material in the form of the Bürgers element (Fig. 4b) was taken into account. The differential constitutive equation of the model material can be written as

$$a_2\sigma_{,tt} + a_1\sigma_{,t} + a_0\sigma = b_2\varepsilon_{,tt} + b_1\varepsilon_{,t}, \tag{7}$$

where

$$a_2=\gamma_1\gamma_2,\quad a_1=(E_1+E_2)\gamma_1+E_1\gamma_2,$$
$$a_0=E_1E_2,\quad b_2=E_1\gamma_1\gamma_2,\quad b_1=E_1E_2\gamma_1. \tag{8}$$

4. Mathematical models of the systems

4.1. Two-parameter model of material

To obtain mathematical description of the viscoelastic beam model one should multiply Eq. (1) with operator Γ. The bending moment M is given

$$M=-EJ_z w_{,xx}-J_z\gamma w_{,xxt}. \tag{9}$$

Using Eqs. (2), (5) and (6) one receives

$$\begin{aligned}&w_{,tt}+2cw_{,xt}+c^2w_{,xx}+\frac{EJ_z}{\rho A_z}w_{,xxxx}+\frac{J_z\gamma}{\rho A_z}w_{,xxxxt}\\&-\frac{P_0}{\rho A_z}w_{,xx}-\frac{3}{2}\frac{E}{\rho}w_{,x}^2w_{,xx}\\&-2\frac{\gamma}{\rho}(w_{,x}w_{,xt}w_{,xx}+cw_{,x}w_{,xx}^2)\\&-\frac{\gamma}{\rho}(w_{,x}^2w_{,xxt}+cw_{,x}^2w_{,xxx})=0.\end{aligned} \tag{10}$$

The boundary conditions

$$w(0,t)=w(l,t)=0,\quad w_{,xx}(0,t)=w_{,xx}(l,t)=0. \tag{11}$$

Let the dimensionless parameters be

$$z=\frac{w}{h_z},\quad \xi=\frac{x}{l},\quad s=\frac{c}{c_f}=c\sqrt{\frac{A_z\rho}{P_0}},$$
$$\tau=t\frac{c_f}{l}=\frac{t}{l}\sqrt{\frac{P}{A_z\rho}},\quad c_f=\sqrt{\frac{P}{A_z\rho}}. \tag{12}$$

The substitution of Eq. (12) into Eq. (10) gives the dimensionless non-linear equation of the viscoelastic beam model motion

$$\begin{aligned}&z_{,\tau\tau}+2sz_{,\xi\tau}+(s^2-1)z_{,\xi\xi}+sz_{,\xi}+\varepsilon z_{,\xi\xi\xi\xi}\\&+\beta z_{,\xi\xi\xi\xi\tau}-\frac{3}{2}\kappa z_{,\xi}^2z_{,\xi\xi}-\eta s(2z_{,\xi\xi}z_{,\xi}+z_{,\xi}^2z_{,\xi\xi\xi})\\&-\eta(2z_{,\xi}z_{,\xi\tau}z_{,\xi\xi}+z_{,\xi}^2z_{,\xi\xi\tau})=0\ \text{where}\end{aligned} \tag{13}$$

$$\beta=\frac{J_z\gamma}{l^3\sqrt{P\rho A_z}},\quad \varepsilon=\frac{EJ_z}{Pl^2}\quad \kappa=\frac{Eh_z^2A_z}{Pl^2},$$
$$\eta=\frac{\gamma h_z^2A_z}{l^3\sqrt{P\rho A_z}}. \tag{14}$$

The problems represented by Eq. (13) together with boundary conditions (11) have been solved using the Galerkin method. The following finite series representation of the dimensionless transverse displacement has been assumed

$$z(\xi,\tau)=\sum_{i=1}^{n}\sin(i\pi\xi)q_i(\tau), \tag{15}$$

where $q_i(\tau)$ is the generalized displacement.

Substituting Eq. (15) into Eq. (13) and using orthogonality condition one determines the set of ordinary differential equations. For $n=3$ the set of ordinary equations is shown in Appendix (Eq. (A.1)).

4.2. Four-parameter model of material

To obtain mathematical description of the system with the four-parameter model of the material one should multiply Eq. (1) with operator Γ and using Eqs. (7) and (8) receives

$$\begin{aligned}&\rho a_0w_{,tt}+2\rho a_0cw_{,xt}+c^2\rho a_0w_{,xx}+\rho a_1w_{,ttt}\\&+3\rho a_1cw_{,xtt}+3\rho a_1c^2w_{,xxt}+\rho a_1c^3w_{,xxx}\\&+\rho a_2w_{,ttt}+3\rho a_2cw_{,xtt}+3\rho a_2c^2w_{,xxt}\\&+\rho a_2c^3w_{,xxt}+a_0r_1w_{,xxxx}+(a_1r_1+a_0r_2)w_{,xxxt}\\&+(a_2r_1+a_1r_2)w_{,xxxtt}+a_1r_1cw_{,xxxx}\\&+c(a_2r_1+a_1r_2)w_{,xxxxt}+a_2cr_2w_{,xxxxtt}\\&+a_2r_2w_{,xxxttt}-\sigma_0w_{,xx}-\sigma_0a_1w_{,xxt}\\&-\sigma_0a_1cw_{,xxx}-\sigma_0a_2w_{,xxtt}-\sigma_0a_2cw_{,xxxt}\\&=2b_1w_{,x}w_{,xx}w_{,xt}+2b_1cw_{,x}w_{,xx}^2\\&+2b_2w_{,x}w_{,xx}w_{,xtt}+2b_2cw_{,x}w_{,xx}w_{,xxt}\\&+b_1w_{,x}^2w_{,xxt}+b_1cw_{,x}^2w_{,xxx}\\&+b_2w_{,x}^2w_{,xxtt}+b_2cw_{,x}^2w_{,xxxt}\end{aligned} \tag{16}$$

where

$$r_1 = \frac{E_0 J_z}{A_z}, \quad E_0 = \frac{E_1 E_2}{E_1 + E_2}, \quad r_2 = \frac{J_z \gamma_2}{A_z},$$

$$\sigma_0 = \frac{P}{A_z}.$$

The boundary conditions are shown in Eq. (11). The substitution of Eq. (12) into Eq. (16) gives the dimensionless non-linear equation of the viscoelastic beam model motion

$$\begin{aligned} & z_{,\tau\tau\tau\tau} + 3s z_{,\xi\tau\tau\tau} + (3s^2 - 1) z_{,\xi\xi\tau\tau} + s(s^2 - 1) z_{,\xi\xi\xi\tau} \\ & \quad + g_1 z_{,\tau\tau\tau} + 3 g_1 s z_{,\xi\tau\tau} + g_1 (3s^2 - 1) z_{,\xi\xi\tau} + g_2 z_{,\tau\tau} \\ & \quad + 2 g_2 s z_{,\xi\tau} + g_2 (s^2 - 1) z_{,\xi\xi} - g_1 s (s^2 - 1) z_{,\xi\xi\xi} \\ & \quad - g_2 g_3 z_{\xi\xi\xi\xi} - (g_1 g_3 + g_2 g_4) z_{\xi\xi\xi\xi\tau} \\ & \quad - (g_3 + g_1 g_4) z_{\xi\xi\xi\xi\tau\tau} - g_1 g_3 s z_{\xi\xi\xi\xi\xi} \\ & \quad - (g_3 + g_1 g_4) z_{\xi\xi\xi\xi\xi\tau} - g_4 s z_{\xi\xi\xi\xi\xi\tau\tau} - g_4 z_{\xi\xi\xi\xi\xi\tau\tau\varsigma} \\ & \quad = g_5 (2 z_{,\xi} z_{,\xi\xi} z_{,\xi\tau} + 2 s z_{,\xi} z_{,\xi\xi}^2 + z_{,\xi}^2 z_{,\xi\xi\tau} \\ & \qquad + s z_{,\xi}^2 z_{,\xi\xi\xi}) + g_6 (2 z_{,\xi} z_{,\xi\xi} z_{,\xi\tau\tau} \\ & \qquad + 2 s z_{,\xi} z_{,\xi\xi} z_{,\xi\xi\tau} + z_{,\xi}^2 z_{,\xi\xi\tau\tau} + s z_{,\xi}^2 z_{,\xi\xi\xi\tau}), \end{aligned} \tag{17}$$

where

$$g_1 = \left(\frac{E_1 + E_2}{\gamma_2} + \frac{E_1}{\gamma_1} \right) \frac{l}{c_f}, \quad g_2 = \frac{E_1 E_2 l^2}{\gamma_1 \gamma_2 c_f^2},$$

$$g_3 = \frac{E_1 J_z}{P l^2}, \quad g_4 = \frac{J_z \gamma_2 c_f}{P l^3},$$

$$g_5 = \frac{E_1 E_2 h_z^2 A^2 c_f \rho}{P^2 \gamma_2 l}, \quad g_6 = \frac{E_1 A h_z^2}{P l^2}. \tag{18}$$

The problems represented by Eq. (17) together with boundary conditions (11) have been solved using the Galerkin method. The finite series representation (15) of the dimensionless transverse displacement has been assumed. Substituting Eq. (15) into Eq. (17) and using orthogonality condition one determines the set of ordinary differential equations. For $n = 3$ the set of ordinary equations is shown in the Appendix (Eq. (A.2)).

5. Numerical results

Numerical investigations have been carried out for the beam model of the steal web. Parameters data: length l=1 m, width b=0.2 m, thickness h=0.0015 m, mass density ρ=7800 kg/m^3, Young's modulus along x: $E_x = 0.2\ 10^{12}$N/m^2, initial stress $N_0 = 2500$ N/m, $n = 3$. Initial conditions: $q_1 = 1$, $q_{1,t} = 0, \ldots, q_{3,ttt} = 0$. The Runge–Kutta method was used to integrate ordinary differential equations and analyze the dynamic behavior of the system.

5.1. Two-parameter model of material

At first, the linearized damped system was investigated. To show the dynamic behavior of the web natural damped oscillations of the first generalized coordinate q_1 for different values of axial speed s of the beam model were investigated. In subcritical region of transport speeds ($s < s_{cr}$) one can observe free flexural damped vibrations around trivial equilibrium position (Fig. 5). In supercritical transport speeds ($s > s_{cr}$) for small internal damping the web experiences divergent instability (Fig. 6) and next flutter instability (Fig. 8). Between these two instability regions there is the second stability domain. The existence of the second stable region is dependent on the internal damping of the web material. When the internal damping increases the width of the second stable region decreases. The time history of the first generalized coordinate q_1 in the second stable region is shown in Fig. 7. The location of instability regions of the linearized system (A.1) with two-parameter model of axially moving material is shown in Fig. 9.

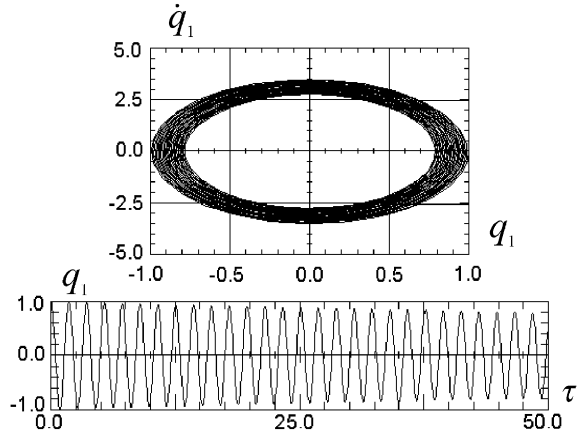

Fig. 5. The phase portrait (a) and time history of the solution of the linearized system (A.1); ($s = 0$, $\beta = 10^{-4}$).

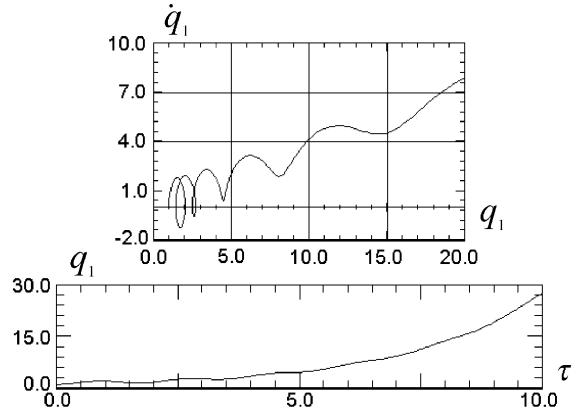

Fig. 6. The phase portrait (a) and time history of the solution of the linearized system (A.1); ($s = 1.4$, $\beta = 10^{-4}$).

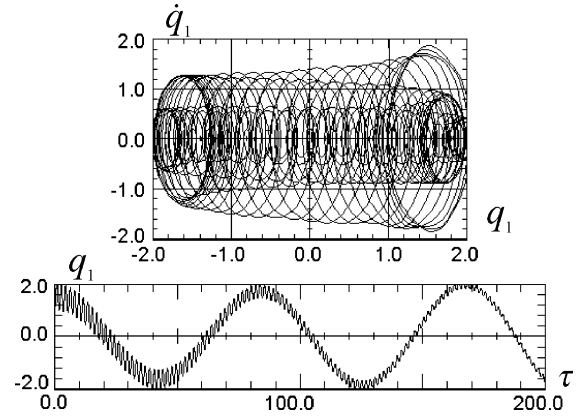

Fig. 7. The phase portrait (a) and time history of the solution of the linearized system (A.1); ($s = 1.41$, $\beta = 10^{-5}$).

Next the non-linear system with the two-parameter model of axially moving material was investigated. Bifurcation diagram of the non-linear system for the internal damping coefficient $\beta = 10^{-5}$ is shown in Fig. 10. The dimensionless transport speed s has been used as the bifurcation parameter. One can observe supercritical bifurcation at the transport speed $s = s_{cr} = 1.12$. For $s < s_{cr}$ only one attractor exists ($q_1 = 0$) and for $s > s_{cr}$ this critical point becomes repaller and one can observe two attractors (non-zero critical points). The phase portraits and time histories of the solutions of the non-linear system (A.1) are shown in Figs. 11–13.

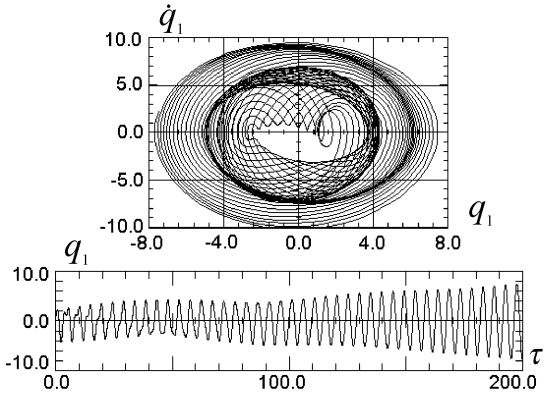

Fig. 8. The phase portrait (a) and time history of the solution of the linearized system (A.1); ($s = 1.45$, $\beta = 10^{-5}$).

It is worth to note that the analysis of the non-linear system does not show the existance of various forms of instability regions of the linearized system (A.1). Though the analysis of the linearized system predicts exponentially growing oscillations in the divergence instability region of transport speeds, non-linear damped oscillations which tend to the stable critical point occur (Fig. 11). At the transport speeds above the first divergence instability region of the linearized system the undamped non-linear system experiences global motion between two critical points (Fig. 12). For different values of internal damping and initial conditions the system may reach various equilibrium positions in the supercritical transport speeds region (Fig. 13).

5.2. Four-parameter model of the material

To allow the direct comparison of the results obtained for the Kelvin–Voigt and Bürgers models in the numerical studies of the second one we used $E_1 = E_2 = 2E$; $\gamma_1 = \gamma_2 = 2\gamma$.

5.2.1. Linearized system

The stability and instability regions calculated for the linearized system (A.2) are shown in Fig. 14. The Bürgers model results indicate that in the range of supercritical transport speed only for smaller values of internal damping coefficient ($\beta < 3 \times 10^{-5}$) the dynamical behavior of the web is similar to the one obtained by the Kelvin–Voigt model (compare with

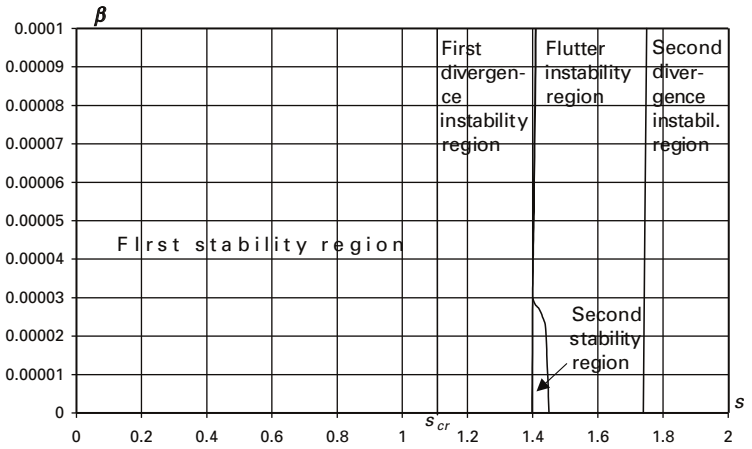

Fig. 9. Instability regions of the linearized system with two-parameter model (Kelvin–Voigt element) of axially moving material .

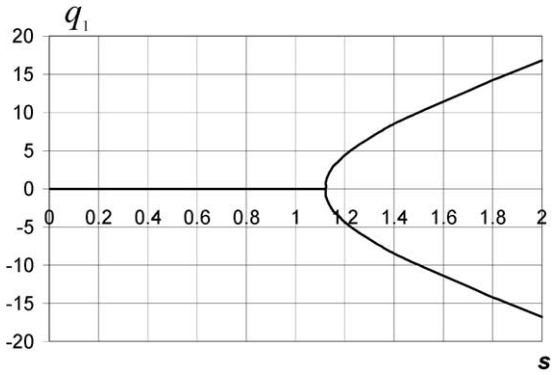

Fig. 10. Bifurcation diagram of the non-linear system with two-parameter model (Kelvin–Voigt element) of axially moving material ($\beta = 10^{-5}$).

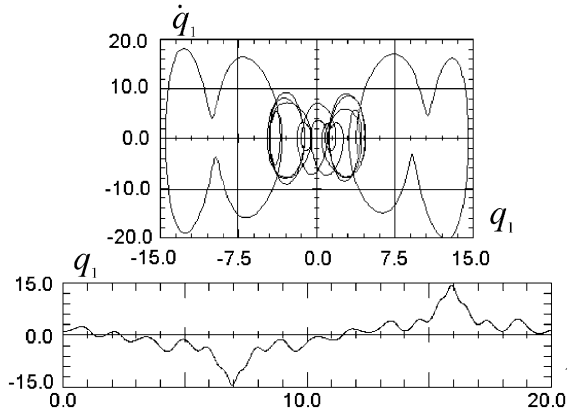

Fig. 12. The phase portrait (a) and time history of the solution of the non-linear system (A.1); ($s = 1.54$, $\beta = 0$).

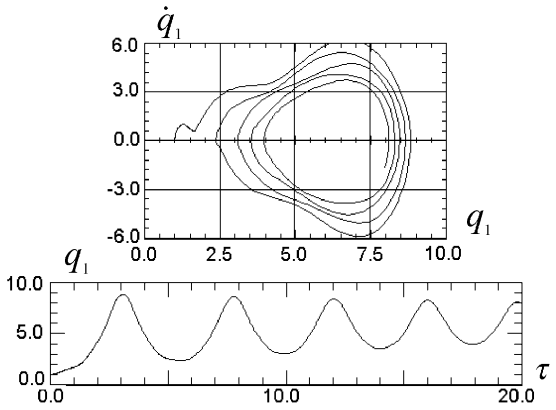

Fig. 11. The phase portrait (a) and time history of the solution of the non-linear system (A.1); ($s = 1.3$, $\beta = 10^{-4}$).

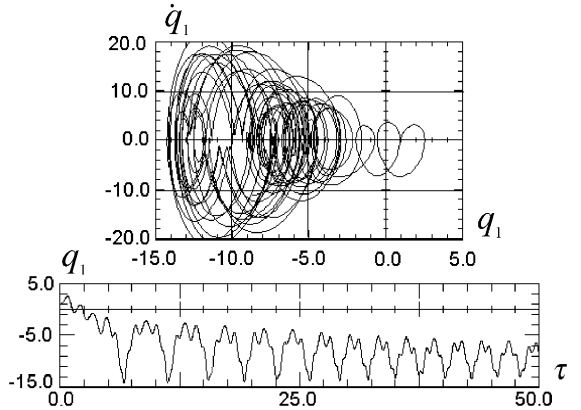

Fig. 13. The phase portrait (a) and time history of the solution of the non-linear system (A.1); ($s = 1.54, \beta = 10^{-5}$).

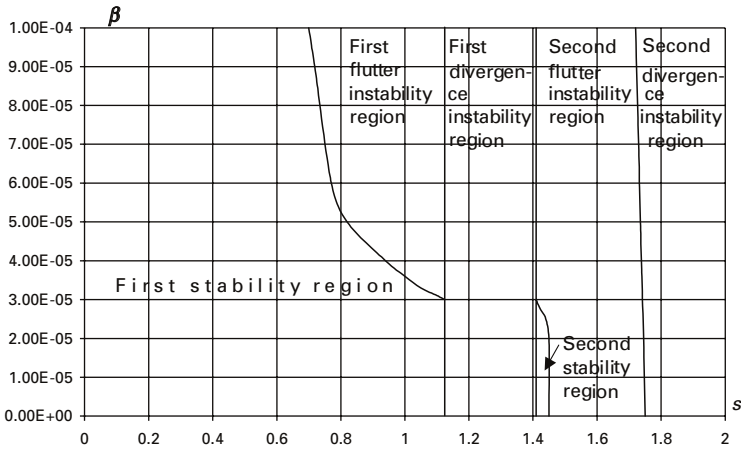

Fig. 14. Instabilities regions of the linearized system with four-parameter model (Bürgers element) of axially moving material.

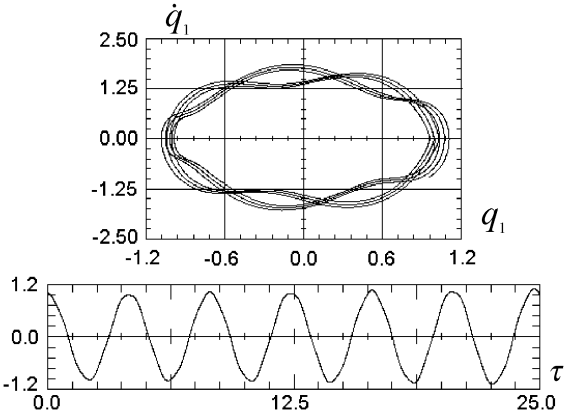

Fig. 15. The phase portrait (a) and time history of the solution of the linearized system (A.2); ($s = 0.93, \beta = 10^{-4}$).

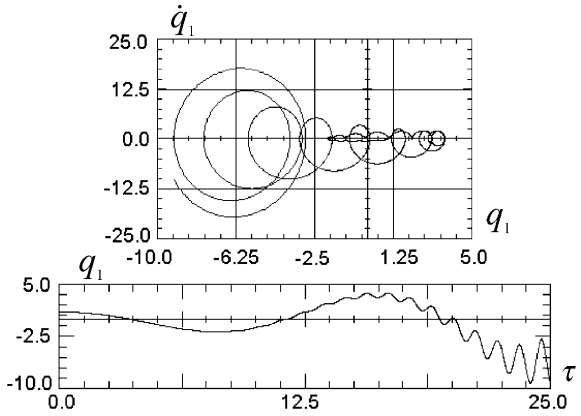

Fig. 16. The phase portrait (a) and time history of the solution of the linearized system (A.2); ($s = 1.1, \beta = 8.9\ 10^{-4}$).

Fig. 9). Both models confirm the existence of the second stability region located between the divergence and the flutter instability regions. Phase portrait and time history of oscillations in this region, are shown in Fig. 17.

For the larger values of internal damping the system loses its stability due to the flutter instability. This is the significant difference between both considered models, as the Kelvin–Voigt model does not allow the identification of this instability region. The critical value of the transport speed decreases with the increase of damping coefficient β. The phase portraits and time histories of the system response in both flutter instability regions are shown in Figs. 15, 16 and 18.

5.2.2. *Non-linear system*

Bifurcation diagram of the non-linear system with four-parameter model of axially moving material for the internal damping coefficient $\beta = 10^{-5}$ is shown in Fig. 19. For $s < s_{cr} = 1.12$ only one attractor exists ($q_1 = 0$).For $s > s_{cr}$ at first one can observe

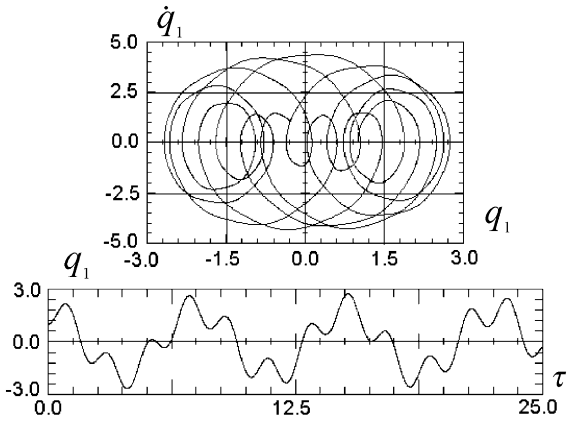

Fig. 17. The phase portrait (a) and time history of the solution of the linearized system (A.2); ($s = 1.43, \beta = 1.8\ 10^{-5}$).

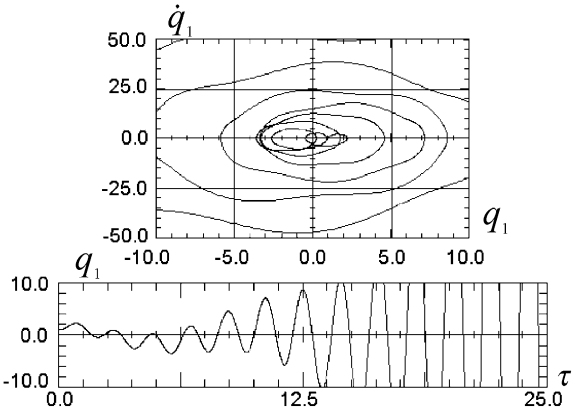

Fig. 18. The phase portrait (a) and time history of the solution of the linearized system (A.2); ($s = 1.42, \beta = 10^{-4}$).

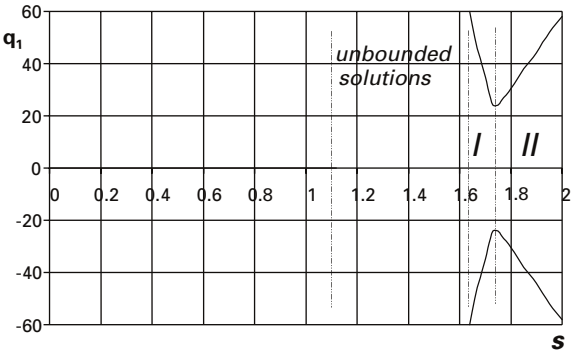

Fig. 19. Bifurcation diagram of the non-linear system with four-parameter model (Bürgers element) of axially moving material ($\beta = 10^{-5}$, I-large limit cycle region, II-small limit cycle region).

the region of transport speeds where unbounded solutions occur. Above this region the non-linear oscillations occur which are characterize by one large limit cycle (region I in Fig. 19). In the second divergence instability region of the linearized system one can observe the non-linear oscillations which are characterize by two small limit cycles (region II in Fig. 19).

The phase portraits and time histories of the system response (the first generalized co-ordinate - q_1) of the non-linear system (A.2) for the small values of internal damping co-efficient ($\beta < 3 \times 10^{-5}$) are shown in Figs. 20–25. Numerical studies of the non-linear

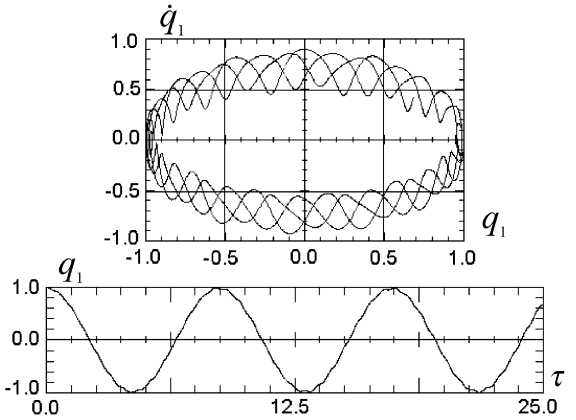

Fig. 20. The phase portrait (a) and time history of the solution of the non-linear system (A.2); ($s = 1,\ \beta = 2\ 10^{-5}$).

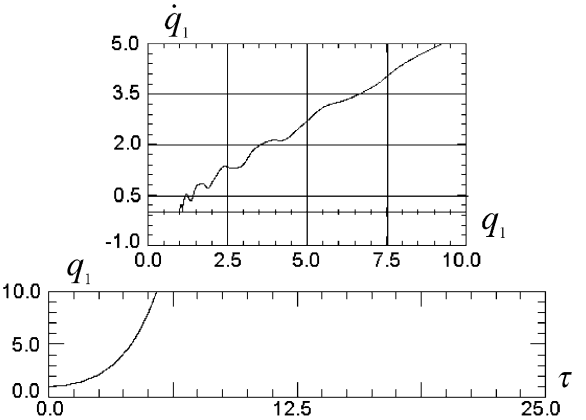

Fig. 21. The phase portrait (a) and time history of the solution of the non-linear system (A.2); ($s = 1.2,\ \beta = 10^{-5}$).

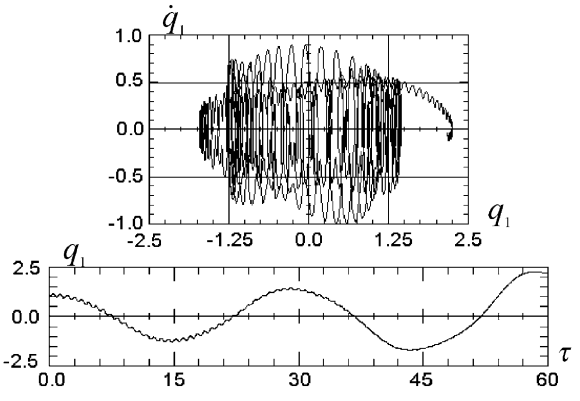

Fig. 22. The phase portrait (a) and time history of the solution of the non-linear system (A.2); ($s = 1.42,\ \beta = 2\ 10^{-5}$).

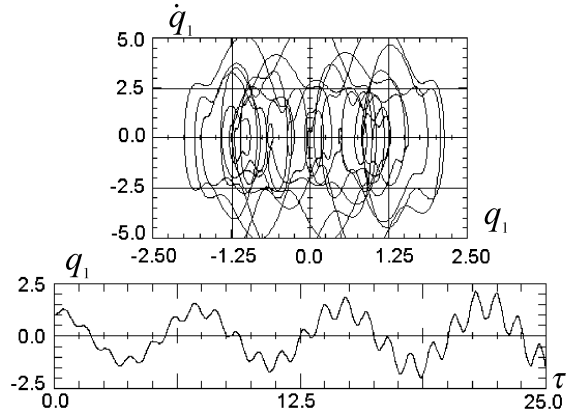

Fig. 23. The phase portrait (a) and time history of the solution of the non-linear system (A.2); ($s = 1.55,\ \beta = 2\ 10^{-5}$).

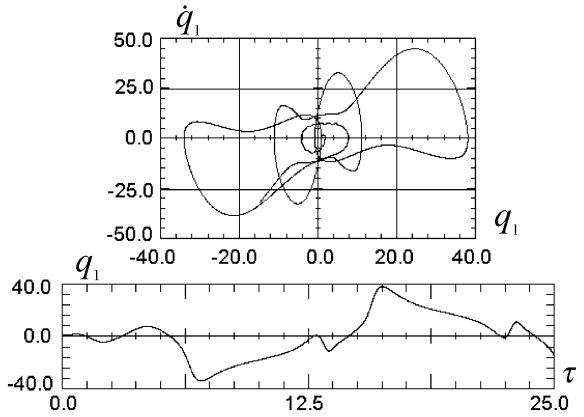

Fig. 24. The phase portrait (a) and time history of the solution of the non-linear system (A.2); ($s = 1.68,\ \beta = 2\ 10^{-5}$).

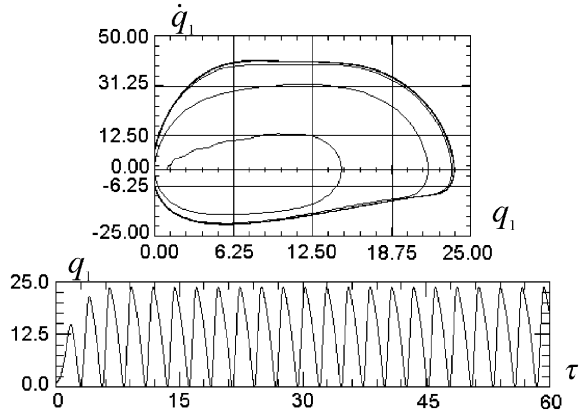

Fig. 25. The phase portrait (a) and time history of the solution of the non-linear system (A.2); ($s = 1.75,\ \beta = 10^{-5}$).

system (A.2) show that in the subcritical range of transport speed s one observes that the increase of s causes the decrease of the frequency of the natural oscillations. At the critical speed the system exhibits the divergent instability (Fig. 21). Compare the previous cases of Kelvin–Voigt (A.1) and linearized Bürgers (A.2) model the existence of the second stability region has not been confirmed (Fig. 22). For larger values of the transport speed one observes the region of flatter instability. The characteristic system response in this region is shown in Fig. 23. With further increase of the transport speed the large limit cycle oscillations around two equilibria are developed (Fig. 24). This type of oscillations is similar to the one observed in Kelvin–Voigt model (Fig. 12). The small limit cycle oscillations can be observed in Fig. 25.

The threshold value of the non-dimensional co-efficient of the internal damping in the case of the considered steel web corresponds to the value of $\gamma = 1.7 \times 10^7\ \mathrm{kgm^{-1}\ s^{-1}}$. The experimental estimations of this co-efficient indicates the larger value $\gamma \approx 10^8\ \mathrm{kgm^{-1}\ s^{-1}}$ [21].

Bifurcation diagram of the non-linear system for the internal damping coefficient $\beta = 10^{-4}$ is shown in Fig. 26. For $s > s_{\mathrm{cr}} = 0.75$ at first the region of transport speeds where unbounded solutions occurs.

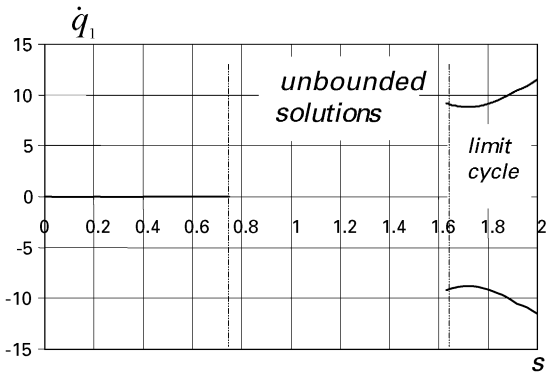

Fig. 26. Bifurcation diagram of the non-linear system with four-parameter model (Bürgers element) of axially moving material ($\beta = 10^{-4}$).

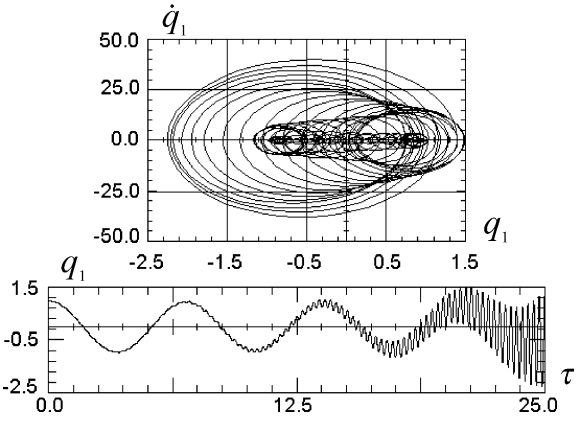

Fig. 27. The phase portrait (a) and time history of the solution of the non-linear system (A.2); ($s = 0.8,\ \beta = 8.9\ 10^{-5}$).

For larger values of the transport speed one observes the co-existing limit cycle oscillations.

The phase portraits and time histories of the system response (the first generalized co-ordinate - q_1) of the non-linear system (A.2) for larger values of internal damping co-efficient ($\beta > 3 \times 10^{-5}$) are shown in Figs. 27–32. At the critical transport speed the system loses the stability due to the flutter instability as it can be seen in Fig. 27. The increase of the transport speed and the transition to the divergence instability region of the linearized system (A.2) do not show the qualitative change of the response character. In this range of transport speed values initially

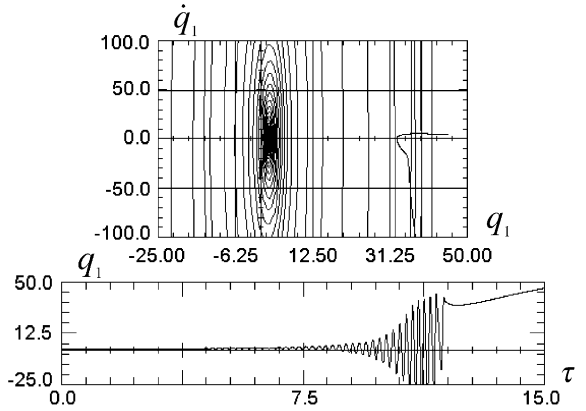

Fig. 28. The phase portrait (a) and time history of the solution of the non-linear system (A.2); ($s = 1.15,\ \beta = 10^{-4}$).

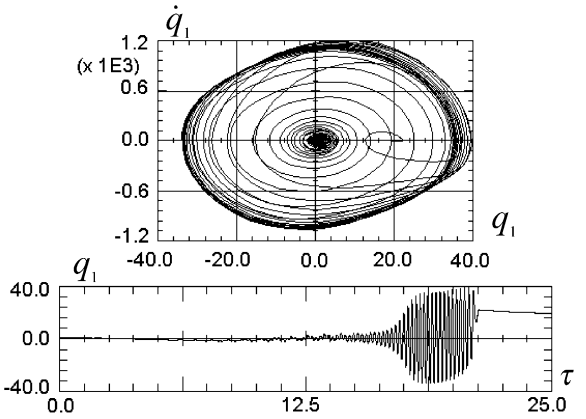

Fig. 29. The phase portrait (a) and time history of the solution of the non-linear system (A.2); ($s = 1.45,\ \beta = 5\ 10^{-5}$).

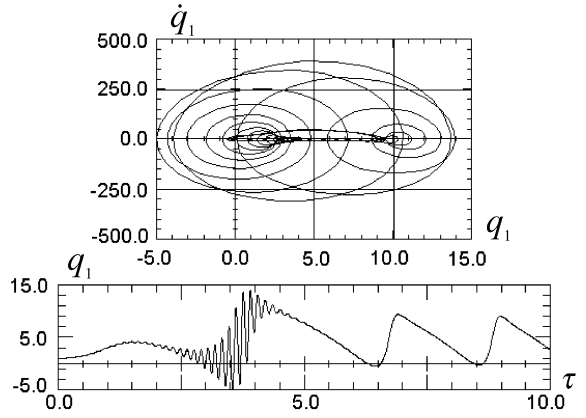

Fig. 30. The phase portrait (a) and time history of the solution of the non-linear system (A.2); ($s = 1.77,\ \beta = 10^{-4}$).

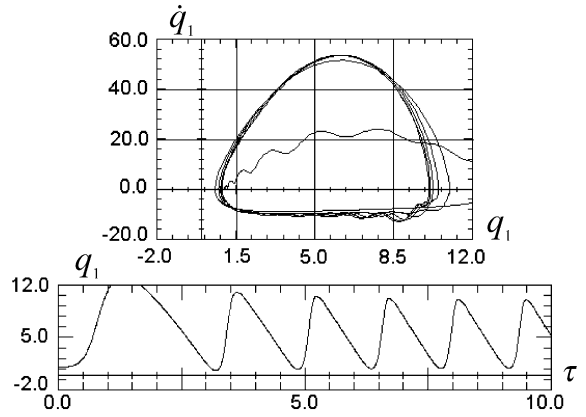

Fig. 31. The phase portrait (a) and time history of the solution of the non-linear system (A.2); ($s = 1.9,\ \beta = 10^{-4}$).

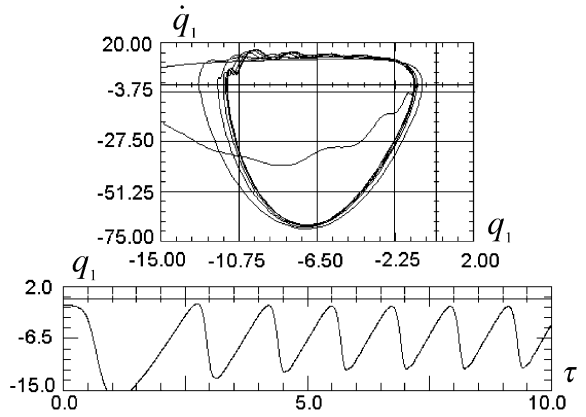

Fig. 32. The phase portrait (a) and time history of the solution of the non-linear system (A.2); ($s = 2.0,\ \beta = 10^{-4}$).

one observes the oscillations with growing amplitude which later are replaced by nonoscillatory increase of the system deflection as can be seen in Fig. 28. Similar dynamical behavior of the non-linear system (A.2) can be observed in the region of flatter instability of the linearized system. In non-linear case the oscillations around the trivial equilibrium ($q_1 = 0$) are replaced by the limit cycle oscillations around noncentral equilibria. The birth of such a limit cycle is shown in Figs. 29 and 30. Phase portraits and time histories of the system response showing the stable limit cycle around two different equilibria are shown in Figs. 31 and 32.

6. Conclusions

Dynamic investigations of beam-like models of the axially moving web with constant axial stress are carried out in this paper. The beam model material as the Kelvin–Voigt element (two-parameter model) and the Bürgers element (four-parameter model) are considered. The general forms of differential equations of transverse oscillations of the systems are derived together with the differential constitutive law for their rheologic models.

The numerical investigations have been carried out for the steal web. The analysis of the linearized equations with two-parameter Kelvin–Voigt material model shows that in the subcritical range of transport speed the increase of this speed causes the decrease of the frequency of the natural oscillations. At critical speed the system exhibits the divergent instability.

For supercritical transport speeds and small internal damping, the web experiences divergent and flutter instabilities. Between these two instability regions there is the second stability area. The width of this region depends on the internal damping of the web material. When the internal damping increases the width of the second stable region decreases more and finally disappears.

The dynamic analysis of the non-linear damped system with constant axial stress shows in supercritical transport speed region the non-trivial equilibrium positions bifurcate from the straight configuration of the web and global motion between the co-existing equilibrium positions occurs. At the same transport speed for different values of the internal damping the system may reach various equilibrium positions.

Four parameters Bürgers model and two parameters Kelvin–Voigt one give dynamically similar results only for small values of the internal damping ($\beta < 3 \times 10^{-5}$). As the experimental estimation of the internal damping in the steel web indicates larger values of β so for the description of the dynamical behavior of such a web one has to consider non-linear Bürgers model. In such a model the critical transport speed decreases with an increase of internal damping and the system loses stability as the result of flutter.

Inside the instability regions one can observe different dynamical behavior depending on the considered model. Non-linear Kelvin–Voigt model shows

the existence of the stable limit cycle in both regions of divergence instability while the non-linear Bürgers model indicates such a behavior only in the second region.

Generally, we can state that results of the non-linear stability analysis simplify the qualitative description of the dynamic behavior of the considered system. Both linear and non-linear stability analysis results coincide at the estimation of the first instability of the system, and differ in the description of the behavior in the unstable region. Numerical studies of Kelvin–Voigt and Bürgers models show that both models give similar results for small values of internal damping and can be used to describe the dynamics of axially moving webs made from materials with internal damping coefficient smaller than 3×10^{-5}. For the materials with larger damping coefficient the Bürgers model is more appropriate.

Appendix A

The set of ordinary differential equations of the viscoelastic beam model with two-parameter Kelvin–Voigt model of material ($n=3$):

$$\begin{aligned}
\ddot{q}_1 &= (s^2-1)\pi^2 q_1 - \varepsilon_z\pi^4 q_1 + (16/3)s\dot{q}_2 - b_z\dot{q}_1 \\
&\quad + (8/3)b_z s q_2 - b_w\pi^4\dot{q}_1 - a_1[(3/8)q_1^3 + 3q_1q_2^2 \\
&\quad + (27/4)q_1q_3^2 + (9/8)q_1^2q_3 + (9/2)q_2^2q_3] \\
&\quad + a_2 s[(848/21)q_1q_2q_3 + (2992/35)q_2q_3^2 \\
&\quad + (112/15)q_1^2q_2 + (1408/105)q_2^3] \\
&\quad - a_2[(3/4)q_1^2\dot{q}_1 + (3/4)q_1^2\dot{q}_3 + (3/2)q_1\dot{q}_1q_3 \\
&\quad + 3q_2^2\ddot{q}_3 + 6q_2\dot{q}_2q_3 + 4q_1q_2\dot{q}_2 \\
&\quad + 2\dot{q}_1q_2^2 + (9/2)\dot{q}_1q_3^2 + 9q_1q_3\dot{q}_3],
\end{aligned}$$

$$\begin{aligned}
\ddot{q}_2 &= 4(s^2-1)\pi^2 q_2 - 16\varepsilon_z\pi^4 q_2 - (16/3)s\dot{q}_1 \\
&\quad + (48/5)s\dot{q}_3 - b_z\dot{q}_2 - (8/3)b_z s q_1 \\
&\quad + (24/5)b_z s q_3 - 16b_w\pi^4\dot{q}_2(\tau) \\
&\quad - a_1[3q_1^2q_2 + 6q_2^3 + 27q_2q_3^2 + 9q_1q_2q_3] \\
&\quad + a_2 s[(8/15)q_1^3 + (44712/385)q_3^3 \\
&\quad + (1952/105)q_1q_2^2 + (1016/35)q_1q_3^2 \\
&\quad + (936/35)q_1^2q_3 + (1568/15)q_2^2q_3] \\
&\quad + a_2[-6q_1q_2\dot{q}_3 - 6q_1\dot{q}_2q_3 - 12q_2^2\dot{q}_2 \\
&\quad - 6\dot{q}_1q_2q_3 - 4q_1\dot{q}_1q_2 - 36q_2q_3\dot{q}_3 \\
&\quad + (27/2)q_1q_3\dot{q}_3 - 2q_1^2\dot{q}_2 - 18q_3^2\dot{q}_2],
\end{aligned}$$

$$\begin{aligned}
\ddot{q}_3 &= 9(s^2-1)\pi^2 q_3 - 81\varepsilon_z\pi^4 q_3 - (48/5)s\dot{q}_2 - b_z\dot{q}_3 \\
&\quad - (24/5)b_z s q_2 - 81b_w\pi^4\dot{q}_3 - a_1[(3/8)q_1^3 \\
&\quad + (243/8)q_3^3 + (9/2)q_1q_2^2 + (27/4)q_1^2q_3 \\
&\quad + 27q_2^2q_3] + a_2 s[-(10656/105)q_1q_2q_3 \\
&\quad + (78192/385)q_2q_3^2 + (144/35)q_1^2q_2 \\
&\quad - (128/15)q_2^3] - a_2[(3/4)q_1^2\dot{q}_1 + (9/2)q_1^2\dot{q}_3 \\
&\quad + 4q_1\dot{q}_1q_2 + (243/4)q_3^2\dot{q}_3 + 9q_1\dot{q}_1q_3 \\
&\quad + 2q_1q_2\dot{q}_2 + 3\dot{q}_1q_2^2 + 18q_2^2\dot{q}_3 + 36q_2\dot{q}_2q_3],
\end{aligned} \tag{A.1}$$

where

$$a_1 = \frac{Eh_z^2A_z\pi^4}{Pl^2}, \quad a_2 = \frac{\gamma h_z^2A_z\pi^4}{l^3\sqrt{PA_z\rho}}.$$

The set of ordinary differential equations of the viscoelastic beam model with four-parameter Bürgers model of material ($n=3$):

$$\begin{aligned}
\dddot{q}_1 &= -(\pi^4g_4 + g_1)\ddot{q}_1 + 8s\ddot{q}_2 - [\pi^2(1-3s^2) + g_2 \\
&\quad + \pi^4(g_3 + g_1g_4)]\ddot{q}_1 + (8g_1s + 128\pi^4g_4s/3)\ddot{q}_2 \\
&\quad - [\pi^2g_1(1-3s^2) + \pi^4(g_1g_3 + g_2g_4)]\dot{q}_1 \\
&\quad + [32\pi^2s(1-s^2)/3 + 16g_2s/3 \\
&\quad + 128\pi^4s(g_3 + g_1g_4)/3]\dot{q}_2 \\
&\quad - [\pi^2g_2(1-s^2) + \pi^4g_2g_3)q_1 \\
&\quad + [32\pi^2g_1s(1-s^2)/3 + 128\pi^4g_1g_3s/3]q_2 \\
&\quad + g_5\pi^4(-3q_1^2\dot{q}_1/8 - 3q_1q_3\dot{q}_1/4 - 3q_2q_3\dot{q}_2 \\
&\quad - 3q_1^2\dot{q}_3/8 - 3q_2^2\dot{q}_3/2 - 2q_1q_2\dot{q}_2 - 9q_1q_3\dot{q}_3/2 \\
&\quad - q_2^2\dot{q}_1 - 9q_3^2\dot{q}_1/4) + g_5\pi^5s(2.13q_2^3 \\
&\quad + 1.19q_1^2q_2 + 6.54q_1q_2q_3 + 40.74q_2q_3^2) \\
&\quad + g_6\pi^4(-3q_1^2\ddot{q}_1/8 - 3q_1q_3\ddot{q}_1/4 - 3q_2q_3\ddot{q}_2 \\
&\quad - 3q_1^2\ddot{q}_3/8 - 3q_2^2\ddot{q}_3/2 - 2q_1q_2\ddot{q}_2 - 9q_1q_3\ddot{q}_3/2 \\
&\quad - q_2^2\ddot{q}_1 - 9q_3^2\ddot{q}_1/4) + g_6\pi^5s(0.17q_1q_2\dot{q}_1 \\
&\quad + 1.09q_2q_3\dot{q}_1 + 1.02q_1^2\dot{q}_2 - 0.87q_1q_3\dot{q}_2 \\
&\quad + 2.13q_2^2\dot{q}_2 + 6.86q_3^2\dot{q}_2 + 6.33q_1q_2\dot{q}_3 \\
&\quad + 6.77q_2q_3\dot{q}_3),
\end{aligned}$$

$$\begin{aligned}\dddot{q}_2 = &-(16\pi^4 g_4 + g_1)\ddot{q}_2 - 8s\ddot{q}_1 + 72s\ddot{q}_3/5\\ &-[4\pi^2(1-3s^2) + g_2 + 16\pi^4(g_3 + g_1 g_4)]\ddot{q}_2\\ &-(8g_1 s + 8\pi^4 g_4 s/3)\ddot{q}_1 - [4\pi^2 g_1(1-3s^2)\\ &+16\pi^4(g_1 g_3 + g_2 g_4)]\dot{q}_2 + (72g_1 s/5\\ &+1944\pi^4 g_4 s/5)\ddot{q}_3 + [216\pi^2 s(1-s^2)/5\\ &+48g_2 s/5 + 648\pi^2 s(g_3 + g_1 g_4)]\dot{q}_3\\ &-[8\pi^2 g_1 s(1-s^2)/3 + 8\pi^4 g_1 g_3 s/3]q_1\\ &-[8\pi^2 s(1-s^2)/3 + 16g_2 s/3\\ &+8\pi^4 s(g_3 + g_1 g_4)/3]\dot{q}_1 - [4\pi^2 g_2(1-s^2)\\ &+16\pi^4 g_2 g_3)q_2 + [216\pi^2 g_1 s(1-s^2)/5\\ &+1944\pi^4 g_1 g_3 s/5)q_3 + g_5\pi^4(-2q_1 q_2\dot{q}_1\\ &-3q_2 q_3\dot{q}_1 - q_1^2\dot{q}_2 - 9q_1 q_3\dot{q}_2 - 6q_2^2\dot{q}_2\\ &-9q_3^2\dot{q}_2 - 3q_1 q_2\dot{q}_3 - 18q_2 q_3\dot{q}_3)\\ &+g_5\pi^5 s(0.08q_1^3 + 18.49q_3^3 + 2.96q_1 q_2^2\\ &+4.64q_1 q_3^2 + 4.26q_1^2 q_3 + 16.64q_2^2 q_3)\\ &+g_6\pi^4(-2q_1 q_2\ddot{q}_1 - 3q_2 q_3\ddot{q}_1 - 3q_1 q_3\ddot{q}_2\\ &-6q_2^2\ddot{q}_2 - q_1^2\ddot{q}_2 - 9q_3^2\ddot{q}_2 - 3q_1 q_2\ddot{q}_3\\ &-18q_2 q_3\ddot{q}_3) + g_6\pi^5 s(0.08q_1^2\dot{q}_1 + 1.09q_1 q_3\dot{q}_1\\ &-1.31q_2^2\dot{q}_1 - 2.14q_3^2\dot{q}_1 + 4.27q_1 q_2\dot{q}_2\\ &-2.68q_2 q_3\dot{q}_2 + 3.17q_1^2\dot{q}_3 + 19.35q_2^2\dot{q}_3\\ &+18.49q_3^2\dot{q}_3 + 6.71q_1 q_2\dot{q}_3),\end{aligned}$$

$$\begin{aligned}\dddot{q}_3 = &-(81\pi^4 g_4 + g_1)\ddot{q}_3 - (72/5)s\ddot{q}_2 - [9\pi^2(1-3s^2)\\ &+g_2 + 81\pi^4(g_3 + g_1 g_4)]\ddot{q}_3 - (72g_1 s/5\\ &+384\pi^4 g_4 s/5)\ddot{q}_2 - [9\pi^2 g_1(1-3s^2)\\ &+81\pi^4(g_1 g_3 + g_2 g_4)]\dot{q}_3 - [96\pi^2 s(1-s^2)/5\\ &+48g_2 s/5 + 384\pi^4 s(g_3 + g_1 g_4)/5]\dot{q}_2\\ &-[9\pi^2 g_2(1-s^2) + 81\pi^4 g_2 g_3)q_3\\ &-[96\pi^2 g_1 s(1-s^2)/5 + 384\pi^4 g_1 g_3 s/5]q_2\\ &+g_5\pi^4(-3q_1^2\dot{q}_1/8 - 3q_2^2\dot{q}_1/2 - 9q_1 q_3\dot{q}_1/2\\ &-3q_1 q_2\dot{q}_2 - 18q_2 q_3\dot{q}_2 - 243q_3^2\dot{q}_3/8 - 9q_1^2\dot{q}_3/4\\ &-9q_2^2\dot{q}_3) + g_5\pi^5 s(-1.36q_2^3 + 0.65q_1^2 q_2\\ &+16.15q_1 q_2 q_3 - 62.31q_2 q_3^2) + g_6\pi^4(-3q_1^2\ddot{q}_1/8\\ &-3q_2^2\ddot{q}_1/2 - 9q_1 q_3\ddot{q}_1/2 - 3q_1 q_2\ddot{q}_2 - 18q_2 q_3\ddot{q}_2\\ &-243q_3^2\ddot{q}_3/8 - 9q_1^2\ddot{q}_3/4 - 9q_2^2\ddot{q}_3)\\ &+g_6\pi^5 s(1.09q_1 q_2\dot{q}_1 - 4.29q_2 q_3\dot{q}_1 - 0.44q_1^2\dot{q}_2\\ &-1.36q_2^2\dot{q}_2 + 13.64q_1 q_3\dot{q}_2 - 21.07q_3^2\dot{q}_2\\ &+6.76q_1 q_2\dot{q}_3 + 36.98q_2 q_3\dot{q}_3),\end{aligned} \tag{A.2}$$

where

$$g_1 = \left(\frac{E_1 + E_2}{\gamma_2} + \frac{E_1}{\gamma_1}\right)\frac{l}{c_f}, \quad g_2 = \frac{E_1 E_2 l^2}{\gamma_1 \gamma_2 c_f^2},$$

$$g_3 = \frac{E_1 J_z}{Pl^2}, \quad g_4 = \frac{J_z \gamma_2 c_f}{Pl^3},$$

$$g_5 = \frac{E_1 E_2 h_z^2 A^2 c_f \rho}{P^2 \gamma_2 l}; \quad g_6 = \frac{E_1 A h_z^2}{Pl^2}.$$

References

[1] K.I. Kovalenko, The effects of external and internal friction on the dynamic stability of bars, J. Appl. Mech. ASME 23 (1959) 239–245.

[2] K.K. Stevens, On the parametric excitation of a viscoelastic column, AIAA J. 12 (1966) 2111–2116.

[3] A.N. Kounadis, Divergence and flutter instability of elastically restrained structures under follower forces, Int. J. Eng. Sci. 19 (1981) 553–562.

[4] A.N. Kounadis, The existence of regions of divergence instability for nonconservative systems under follower forces, Int. J. Eng. Sci. 19 (1983) 725–733.

[5] J.D. Jin, Y. Matsuzaki, Bifurcations in a two degree of freedom elastic system with follower forces, J. Sound Vibration 126 (2) (1988) 265–277.

[6] W. Altman, M. Goncalves de Oliveira, Vibration and stability of shell panels with slight internal dumping under follower force, J. Sound Vibrations 136 (1) (1990) 45–50.

[7] M.A. De Rosa, C. Franciosi, The influence of an intermediate support on the stability behaviour of Cantilever beams subjected to follower force, J. Sound Vibrations 137 (1) (1990) 107–115.

[8] W. Kurnik, M. Pękalak, Stability, bifurcation analysis of the non-linear damped Leipholz column, J. Sound Vibration 152 (2) (1992) 285–294.

[9] K. Czołczyński, K. Marynowski, Instabilities of the elastically supported laval rotor subjected to a longitudinal force, J. Sound Vibrations 154 (2) (1992) 281–288.

[10] K. Marynowski, K. Czołczyński, T. Kapitaniak, Instabilities of the visco-elastic rotor subjected to a follower force, J. Sound Vibration 180 (2) (1995) 362–367.

[11] W.Z. Wu, C.D. Mote Jr, Parametric excitation of an axially moving band by periodic edge loading, J. Sound Vibration 110 (1) (1986) 27–39.

[12] S.J. Hwang, N.C. Perkins, Supercritical stability of an axially moving beam, Part I, II, J. Sound Vibration 154 (3) (1992) 381–409.
[13] J.A. Wickert, Non-linear vibration of a traveling tensioned beam, Int. J. Non-Linear Mech. 27 (3) (1992) 503–517.
[14] J.A. Wickert, Analysis of self-excited longitudinal vibration of a moving tape, J. Sound Vibration 160 (3) (1993) 455–463.
[15] S.J. Hwang, N.C. Perkins, High speed stability of coupled band/wheel systems: theory and experiment, J. Sound Vibration 169 (4) (1994) 459–483.
[16] J. Moon, J.A. Wickert, Non-linear vibration of power transmission belts, J. Sound Vibration 200 (4) (1997) 419–431.
[17] R.-F. Fung, J.-S. Huang, Y.-C. Chen, C.-M. Yao, Non-linear dynamic analysis of the viscoelastic string with a harmonically varying transport speed, Computers & Structures 66 (6) (1998) 777–784.
[18] R.G. Parker, Supercritical speed stability of the trivial equilibrium of an axially moving string on an elastic foundation, J. Sound Vibration 221 (3) (1999) 205–219.
[19] L. Zhang, J.W. Zu, Non-linear vibration of parametrically excited moving belts, Part I, II, J. Appl. Mech. 66 (2) (1999) 396–409.
[20] K. Marynowski, Non-linear vibration of axially moving orthotropic web, Mech. Mech. Eng. 4 (2) (1999) 131–136.
[21] Z. Osiński, Tłumienie drgań, PWN Warszawa 1997 (in Polish).
[22] A.E.H. Love, The Mathematical Theory of Elasticity, University Press, Cambridge, 1927.
[23] A.M. Freudenthal, H. Geiringer, The Mathematical Theories of the Inelastic Continuum, Encyclopaedia of Physics, Vol. VI, Elasticity and Plasticity, Springer, Berlin-Gőttingen-Heidelberg, 1958.
[24] J.A. Wickert, C.D. Mote Jr., Classical vibration analysis of axially-moving continua, J. Appl. Mech. ASME 57 (1990) 738–744.